Available online at www.sciencedirect.com
SCIENCE DIRECT®
Journal of Nuclear Materials 337–339 (2005) 40–44
journal of nuclear materials
www.elsevier.com/locate/jnucmat

Modelling of deposition of hydrocarbon films underneath the divertor and in the pumping ducts of ITER

G. Federici [a,*], M. Mayer [b], G. Strohmayer [a], V. Chuyanov [a], C. Day [c]

[a] *ITER, JWS Garching Co-center, Boltzmannstraße 2, 85748 Garching, Germany*
[b] *Max-Planck-Institut für Plasmaphysik, EURATOM Association, Boltzmannstraße 2, 85748 Garching, Germany*
[c] *Forschungszentrum Karlsruhe, P.O. Box 3640, 76021 Karlsruhe, Germany*

Abstract

This paper presents the results of a modelling study conducted to estimate the deposition of hydrocarbon radicals in the regions of the ITER divertor hidden from the plasma (e.g., underneath the private flux region dome and in the pumping ducts). A Monte-Carlo code based on the approach described in Ref. [M. Mayer et al., J. Nucl. Mater. 313–316 (2003) 429] has been developed and applied for the actual ITER geometry. It allows for a full 3-dimensional treatment of particle trajectories and follows individual hydrocarbon particles until they either stick on the surfaces or leave the system. The cases analysed clarify the influence of several parameters such as the sticking coefficient of the hydrocarbon species, the pressure of the background gas, and the geometry. Consistent with experimental findings from tokamaks, this assessment shows that particles with relatively high sticking probability (>0.01) deposit primarily underneath the divertor structure, and only species with very small sticking probability ($\leqslant 10^{-3}$) may reach and stick along the inner surfaces of the pumping ducts.

PACS: 07.05.T; 02.50.N; 52.40.H; 81.15
Keywords: Carbon-based materials; Divertor; ITER; Co-deposition; Tritium

1. Introduction

A key decision for the construction and operation of ITER is the choice of plasma-facing materials. Their selection is a compromise between multiple requirements derived from the unique features of a burning plasma environment [2]. Currently, the ITER design contemplates the use of carbon fibre composite (CFC) near the divertor strike points, W elsewhere in the divertor and Be on the main chamber wall [3].

The use of CFC follows directly from the expected material damage for the projected levels of thermal loads during plasma thermal transients (e.g., type I ELMs and disruptions) near the strike points. Tungsten is planned as a possible alternative material for the divertor high heat flux areas. The plasma–material interaction (PMI) issues are reviewed in [4]. Although the current material choice is seen as a compromise to satisfy the often-conflicting requirements, it is known to have unwanted features, which introduce problems. One of the most

* Corresponding author. Tel.: +49 89 32994228; fax: +49 89 32994110.
E-mail address: federig@ipp.mpg.de (G. Federici).

0022-3115/$ - see front matter © 2004 Elsevier B.V. All rights reserved.
doi:10.1016/j.jnucmat.2004.10.007

notable, for example, is that erosion and re-deposition of C-based materials during normal operation and off-normal events will lead, during tritium operation, to T-co-deposition, and efficient methods would be required for its removal to control tritium uptake in the co-deposited films [5].

This paper presents the results of a modelling study conducted to estimate the deposition of hydrocarbon radicals in the regions of the ITER divertor hidden from the plasma (e.g., underneath the private flux region dome and in the pumping ducts). The organisation of this paper is as follows: in Section 2, we briefly discuss the model for film growth. Selected results of parametric analyses are discussed in Section 3. The main uncertainties and future work are briefly described in Section 4, followed by concluding remarks in Section 5.

2. Modelling carbon deposition in ITER shaded regions

2.1. Background

Deposition in the remote areas of the ITER divertor is expected to occur because of the sticking of hydrocarbon radicals. Hydrocarbon radicals with high sticking probability (e.g., C, CH) would lead to film formation in areas of 'first bounce', i.e., near the divertor leg, or underneath the divertor dome. The large amount of hydrocarbon film deposits found in shaded regions of the inboard JET divertor (e.g., the cold louvres in front of the pumping duct) was explained by re-deposition of C_2H_x species [6]. Less reactive species, with much lower sticking probability, like CH_2, CH_3 and C_2H_5 would instead survive many wall collisions (of the order of 10^2–10^4) and migrate long distances, and can be deposited at regions very remote from the source (e.g., the surfaces of the divertor cassette and pumping ducts) [7,8].

2.2. Model description

A Monte-Carlo code based on the approach described in [1] has been developed and applied for the actual ITER geometry. It allows for a full 3-dimensional treatment of particle trajectories and follows individual hydrocarbon particles until they either stick on the surfaces or leave the system. The geometry of the model is shown in Fig. 1. It consists of a ring of 54 divertor cassettes and 4 pumping ducts. No net conductance is assumed between adjacent cassettes, but the implication of this assumption on the results is expected to be negligible. 2 cryopumps are located at the end of each pumping duct (one directly installed at the end of the duct, the other branched) [9]. The simplified model used for this study consists of 4 regions combined together with appropriate boundary conditions. Main geometrical features of the model and assumptions are described in Table 1.

2.3. Main assumptions and calculation procedure

The code assumes the following:

(1) Fully 3-dimensional treatment of particle trajectories.
(2) Particles can enter the system only from region 1. Instead particles can leave the system either from the end of the duct (region 4) i.e., they get pumped, or they can be reflected back into the plasma (region 1).
(3) Particles enter equi-partitioned over the entrance area (wide slots in the upper parts for circulating/pumping neutrals). The initial velocity components are distributed according to a solid angle weighted cosine distribution.
(4) If particles hit a wall, they can either stick, with probability s, or they can be reflected, with probability $1 - s$. Particles are reflected with a solid angle

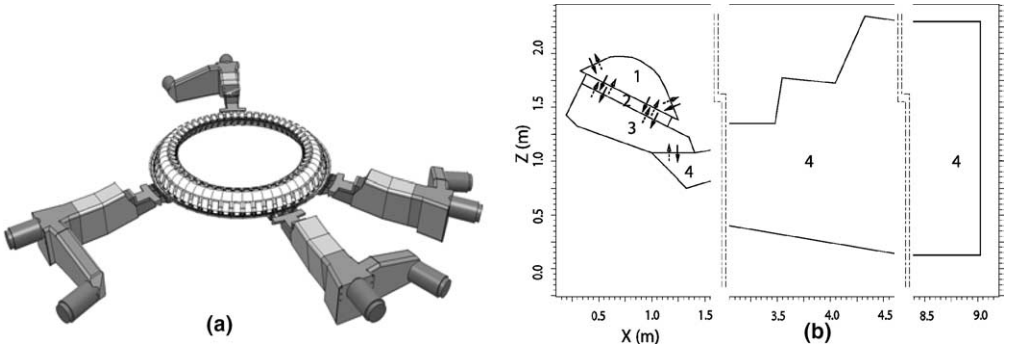

Fig. 1. (a) 3D view of the ITER exhaust gas pumping port geometry showing the branched and direct cryopumps. (b) Poloidal cross-section of the model showing the various regions referred to in Table 1.

Table 1
Main geometry features and assumptions of the model showed in Fig. 1(b) (N_a = 54/4)

Model zones	Particle input (I)/output (O)
Region 1: N_a dome elements connected in toroidal direction, located in the plasma private region, with wide opening slots in the upper parts for circulating/pumping neutrals, and narrow parallel radial slots in the lower part	I: particles enter from the plasma side and from surrounding region 2 (reflected) O: particles leave to go back to the divertor leg or move to region 2
Region 2: N_a divertor trails with narrow parallel radial slots of given width. They connect model region 1 with model region 3	I: particles enter from region 1 or region 3 (reflected) O: particles leave to go back to region 1 or move to region 3
Region 3: Sub-divertor area, which consists of a toroidal ring, bounded at the upper part by the divertor trails and at the bottom part by the lower part of the vacuum vessel. Connect model region 2 with region 4	I: particles enter from region 2 or region 4 (reflected) O: particles leave to go back to region 2 or move to region 4
Region 4: Pumping duct	I: particles enter only from region 3. When they reach the end of the duct they are assumed to be lost to the pumps O: particles leave to go back to region 3 or go to the cryopumps

weighted cosine distribution, i.e. $p(\vartheta) \propto \sin(\vartheta)\cos(\vartheta)$, where ϑ is the angle towards the surface normal. The random number generator creating this distribution is obtained from $\vartheta = \arcsin(\sqrt{x})$, where x is a random number equally distributed in $0, \ldots, 1$. We assume that the sticking onto surfaces undergoing deposition does not vary with time. However, the sticking coefficients that we used for the simulations [10] have been measured in laboratories on surfaces that were already covered with a thin film of amorphous carbon. Thus, they are not far from representing realistic conditions, which will likely occur on stainless steel after onset of deposition. Further work is clearly needed (see Section 4) to assess the impact of this assumption.

(5) The mean-free path can be estimated as follows [11]:

$$\bar{\lambda} = \frac{K_B T}{\sqrt{2} \cdot \pi \cdot \sigma_{ij}^2 p},$$

where K_B is the Boltzmann's constant and T, p are the gas temperature and pressure, respectively. σ_{ii} is the collision diameter of the diffusing species. When $i \neq j$, $\sigma_{ij} = 0.5 \cdot (\sigma_i + \sigma_j)$. For the cases of interest here, the pressure is in the range 1–10 Pa, resulting in mean free path lengths for hydrogen molecules of 0.9–9 mm at room temperature (1.2–12 mm at 423 K). As this is smaller than the characteristic dimensions of the geometry, collisions with gas molecules have to be taken into account. This is done as follows. During each step the free flight path λ of the radical molecule is obtained from $p(\lambda) = \exp(-\lambda/\bar{\lambda})$. The random number generator for this distribution is given by $\lambda = -\bar{\lambda}\ln(1-x)$, where x is a random number equally distributed in $[0, \ldots, 1]$. At the end of the free flight path the radical collides with a D_2 molecule. The radical and the D_2 molecule have velocities according to the Maxwell–Boltzmann distribution. We assume a hard ball potential between the two molecules, and the scattering angle φ is given in the centre of mass system by $\varphi(b) = \arccos(b/(r_1 + r_2))$, where b is the impact parameter, $r_1 = 1.4$ Å the radius of the D_2 molecule, and r_2 is the radius of the radical molecule (see Table 2). The mass of the radical species is listed in Table 2. The probability distribution for b is given by $p(b) = 2b/R^2$, where $R = r_1 + r_2$ and $0 \leqslant b \leqslant R$. This is the probability to hit a circular disk at radius b.

The simulation proceeds schematically as follows. A flux of radicals with a given sticking coefficient is directed towards the entrance of region 4. In general, the

Table 2
Assumed properties of sticking radicals [10]

Species	Sticking coefficient[a]	Atomic mass (Amu)	Molecular radius[b] (10^{-10} m)
(1) CT_3	10^{-4}	21	1.88
(2) C_2T_5	10^{-3}	39	2.22
(3) CT_3+H	10^{-2}	21	1.88
(4) C_2T_3	>0.1	33	2.09
(5) C_2T	0.9	27	2.02

[a] Assuming $s = \beta$.
[b] Assuming $r_i = 0.5 \cdot \sigma_i$.

flux of radicals incident on the divertor consists of an arbitrary mix of C_xH_y or H(D,T). In the calculations presented here the flux is specified as a part of a parametric survey and is assumed to consist of only a single species. However, the distribution of radicals could be specified from experimental measurements (not yet available). We assume a gas in thermal equilibrium with the divertor structures at ~120 °C. The boundary condition at the end of region 4 is that all the particles that cross this boundary moving in an outward direction are lost. An impinging particle at the entrance of region 4 can either collide with the gas molecules (and as a result of this collision(s) its original direction is changed (see below)), or reach a surface without collisions. At the surface the particle can either stick with a probability, which is given by the assumed, sticking coefficient or be reflected. The direction of the reflected radical is determined by the choice of a random number and is distributed according to a solid angle weighted cosine distribution. Each reflected particle can impinge on the wall or collide again with a molecule of the background gas. It is followed until it sticks or leaves the system. The result of this simulation provides the number of particles reflected at the entrance of region 4, those that are sticking, and finally those that reach the pump. To obtain good statistics and eliminate fluctuations, at least $N = 10^5$ particles are required. Then the analysis proceeds with region 3. The calculated number of particles reflected from the entrance of region 4 provides the boundary condition at the end of region 3. The number of particles (out of 10^5) reflected at the entrance of region 3 and sticking are calculated. And so forth for region 2 and 1. The actual number of particles crossing the various boundaries is then scaled based on the calculated number of particles.

3. Results of the calculations and discussion

Fig. 2 shows the calculated fractions of particles: (i) reflected from region 1, (ii) sticked in the different regions, and (iii) pumped. The results are plotted for different values of assumed sticking coefficient for a pressure of 1 Pa (Fig. 2(a)) and 10 Pa (Fig. 2(b)), respectively.

The cases analysed show that, in agreement with experimental findings available from tokamaks (see for example [1,7]), for particles with relatively high sticking probability ($\gg$0.001) deposition occurs primarily underneath the divertor structure, and only species with very small sticking probability (~0.001) may reach and stick along the inner surfaces of the pumping ducts. The deposition pattern along the pump duct (region 4) is shown for the pressure of 1 Pa in Fig. 3 for different sticking probabilities. The results are normalised to a factor: $\varphi_{in} = 10^5$ particles/0.22 $m^2 = 4.6 \times 10^5$ particles/m^2. Once the hydrocarbon flux entering the divertor private region is know, the deposition rate can be simply obtained by scaling the plots by the ratio of the actual flux divided by φ_{in}. One should notice that the deposition pattern for the various species in region 4 is affected by the sticking (e.g., the lower is the sticking the longer is the migration along the duct) and by reflection in regions of the model closer to the plasma (e.g., the lower is the sticking the higher is the fraction of particle reflected back).

The typical path that a particle undergoes in the pump duct before sticking is shown in the insets for a case with low sticking ($s = 0.01$) and a case with relatively high sticking ($s = 0.1$). Based on this study, it can be concluded that only a moderate, but not negligible fraction of low sticking radicals, such as CH_3 can reach the pumping duct.

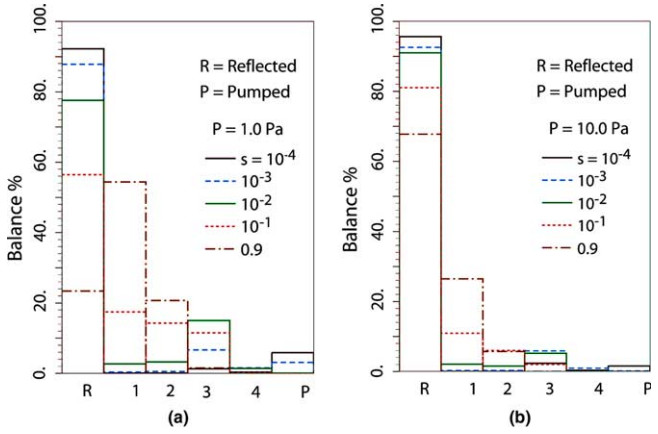

Fig. 2. Deposition in the various regions of the model for different sticking coefficients and different gas pressures. Particles leaving the system at the entrance (reflected) and exhausted at the pumps are also shown. Case (a) 1 Pa; Case (b) 10 Pa.

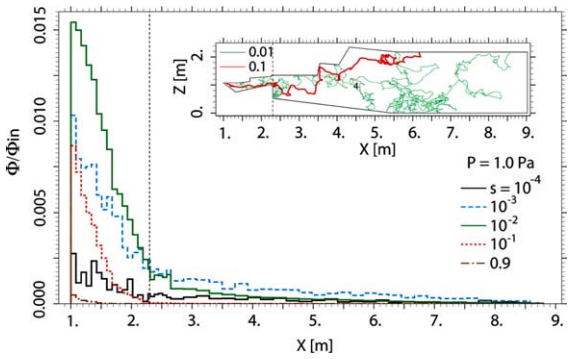

Fig. 3. Deposition pattern along the duct for different sticking coefficients and a gas pressure of 1 Pa. The inset shows the migration path of a particle in region 4 until it sticks for two representative cases with low (0.01) and high (0.1) sticking. (Normalization factor: $\varphi_{in} = 10^5$ particles/0.22 $m^2 = 4.6 \times 10^5$ particles/m^2.)

4. Main uncertainties and future R & D priorities

This assessment clarifies the influence of various parameters (e.g., pressure, composition of exhaust and sticking of characteristic species, geometry) on the deposition pattern and rate in the regions of the ITER divertor hidden from the plasma. The knowledge of these quantities from the operation of existing tokamaks and the extrapolation to ITER are still uncertain in large part due to the difficulty of the associated measurements. We plan to include at a later stage in the model: (i) erosion of the growing films due to atomic hydrogen; (ii) effect of temperature and atomic hydrogen flux on sticking; (iii) gas phase reactions of C_xH_y radicals; (iv) effects of pressure variations and gas flow; and (v) reactions at the walls resulting in loss of radicals (e.g., $CH_3 \rightarrow CH_4$) could be easily included in the model, but have been neglected due to unknown relative probabilities. This, together with further experiments in tokamaks and laboratories (see for example [12]) hopefully would lead to an improvement of understanding.

5. Conclusive remarks

In this paper we discuss the results of a modelling study to simulate the growth of hydrogenated amorphous films in the regions of the ITER divertor hidden from the plasma when the radical fluxes are specified as a part of a parametric survey. We find that, in agreement with experimental findings in some of the existing tokamaks [1,7] most of the radical species entering the divertor private regions will stick on the nearby surfaces (i.e., underneath the dome or in the sub-divertor region). Only a small fraction of low sticking probability species can enter the pumping duct and almost all species except those with very low sticking probabilities ($\leqslant 10^{-3}$) do not reach the pump. Although uncertainties rule out providing firm quantitative predictions, the results of this study are useful to illustrate trends. Further modelling work is planned to take into account effects of parameters such as temperature of the substrate on sticking, re-erosion induced by atomic hydrogen, gas flow, etc., now neglected for sake of simplicity.

Acknowledgments

The authors wish to acknowledge the useful discussion with Drs A. Kirschner and M. Meier. This report was prepared as an account of work undertaken within the framework of ITER Transitional Arrangements (ITA). These are conducted by the European Atomic Energy Community, Japan, the People's Republic of China, the Republic Korea, the Russian Federation, and the United States of America under the auspices of the International Atomic Energy Agency. The views and opinions expressed herein do not necessarily reflect those of the Participants to the ITA, the IAEA or any agency thereof. Dissemination of the information in this paper is governed by the applicable terms of the former ITER-EDA Agreement.

References

[1] M. Mayer et al., J. Nucl. Mater. 313–316 (2003) 429.
[2] G. Federici et al., Selection of plasma-facing materials in next-step fusion devices, 19th Symposium on Fusion Engineering, SOFE, 22–25 January 2002, Atlantic City, New Jersey.
[3] M. Shimada et al., these Proceedings. doi:10.1016/j.jnucmat.2004.09.063.
[4] G. Federici, C.H. Skinner, et al., Nucl. Fusion 41 (2001) 1967.
[5] C.H. Skinner, J.P. Coad, G. Federici, Phys. Scr. T 111 (2004) 92.
[6] A. vonKeudell, C. Hopf, T. Schwarz-Selinger, W. Jacob, Nucl. Fusion 39 (1999) 1451.
[7] V. Rohde et al., J. Nucl. Mater. 313–316 (2003) 337.
[8] J. von Seggern, A. Kirschner, V. Philipps, P. Wienhold, Phys. Scr. T 111 (2004) 118.
[9] Chr. Day et al., R&D progress for the ITER vacuum pumping system, 20th Symposium on Fusion Engineering, SOFE, October 2003, San Diego, California.
[10] C. Hopf, T. Schwarz-Selinger, W. Jacob, A. von Keudell, J. Appl. Phys. 87 (2000) 2719.
[11] R. Cunningham, R. Williams, Diffusion in Gases and Porous Media, Plenum, New York, 1980.
[12] A. Gorodetsky et al., these Proceedings. doi:10.1016/j.jnucmat.2004.09.133.